Solvent-Controlled Spatial Distribution of SI-AGET-ATRP Grafted Polymers in Lignocellulosic Materials

Solvent-Controlled Spatial Distribution of SI AGET ATRP Grafted Polymers in Lignocellulosic Materials

Journal:	*Biomacromolecules*
Manuscript ID	bm-2018-013932.R1
Manuscript Type:	Article
Date Submitted by the Author:	14-Nov-2018

Complete List of Authors:	Vidiella del Blanco, Marta; Eidgenossische Technische Hochschule Zurich, Gomez, Vera; Eidgenossische Technische Hochschule Zurich, IFB Keplinger, Tobias; Eidgenossische Technische Hochschule Zurich, Wood Materials Science Morales, Luiz; Eidgenossische Technische Hochschule Zurich Cabane, Etienne; Eidgenossische Technische Hochschule Zurich, IFB

Solvent-Controlled Spatial Distribution of SI-AGET-ATRP Grafted Polymers in Lignocellulosic Materials

*Marta Vidiella del Blanco, Vera Gomez, Tobias Keplinger, Luiz Fernando Grafulha Morales, and Etienne Cabane**

M. Vidiella del Blanco, V. Gomez, Dr. T. Keplinger, Dr. E. Cabane
Wood Materials Science, ETH Zürich, Stefano-Franscini-Platz 3, 8093 Zürich, Switzerland
and
Applied Wood Materials, EMPA – Swiss Federal Laboratories for Materials Science and Technology, Überlandstrasse 129, 8600 Dübendorf, Switzerland
E-mail: cabanee@ethz.ch

L.F. G. Morales

Scientific Centre for Optical and Electron Microscopy (ScopeM), ETH Zürich, Auguste-Piccard-Hof 1, 8093 Zürich, Switzerland

KEYWORDS: lignocellulosic materials, SI-AGET-ATRP, grafting from, hierarchical structures, cellulose, polymer spatial distribution

ABSTRACT

In the current quest for the design of advanced complex materials, the functionalization of biological materials having hierarchical structures has been of high interest. In the case of lignocellulosic materials, various modification techniques have allowed to obtain materials with outstanding properties. However, the control over the spatial distribution of the modification inside the wood scaffold, which is an important parameter to obtain the desired properties, has yet to be understood. In this study, the use of solvents with different wood-swelling capabilities is proposed to control the spatial polymer-modification distribution inside the hierarchical wood structure. Wood cubes were functionalized via SI-AGET-ATRP using solvents with different wood-swelling capabilities. Spectroscopic (Raman and FTIR) and electron microscopy techniques showed that a good wood-swelling solvent as reaction media can transport the polymerization initiator molecule into the cell wall, allowing it to react with all the available -OH groups in the wood structure. Conversely, the use of a bad wood-swelling solvent limits the reaction to the available -OH groups at the lumen/cell wall interface. The subsequently added polymers grow from the available initiator sites and therefore show similar spatial distribution. This diffusion limitation is visible not only at the microscopic level (cellular structure) but also at the macroscopic level (over the length of the sample).

INTRODUCTION

Design principles inspired by nature are helping to manufacture new advanced materials with superior properties.[1–3] In particular, researchers have paid more and more attention to the complex hierarchical structures found in various biological materials. As shown by numerous recent publications, wood and wood-based materials have attracted a lot of interest in the materials science community.[4–16]

In most of these works, the wood structure is maintained and a chemical modification is needed to introduce new functionalities. Indeed, the properties of new wood-based materials can be greatly enhanced by the introduction of chemical compounds with specific functionalities. There exists a wide variety of chemistries to modify lignocellulosic materials.

The chemicals incorporated into the wood structure can be covalently bonded to the available -OH groups in the wood cell wall polymers. A long list of chemical functionalities have been used to modify wood through covalent bonding with the -OH groups, which include but are not limited to, anhydrides, acyl chlorides, carboxylic acids, isocyanates, aldehydes, lactones, nitriles, epoxides, and DMDHEU (dimethylol dihydroxyethyleneurea).[12,17–20]

Wood may also be functionalized through the grafting of polymer chains.[14,17,21–23] Polymers are of special interest as they can provide wood with a higher variety of functional groups, when compared to modification by a single molecule. In addition to their chemical diversity, polymer properties depend on other parameters such as polymer chain length, polymer composition (copolymers), polymer architecture (linear, branched, star …), which may also contribute to the final properties of the wood-polymer composite.

Besides considerations on the physicochemical properties of the modifying agents, a key parameter is their spatial distribution inside the wood structure. Wood is an anisotropic porous material with a hierarchical arrangement over several length scales. Therefore, regardless of the type of chemistry employed, the chemicals will reach different regions in the wood scaffold. At the microscale (cell and cell wall level), distribution of the modification may essentially target the lumen, the lumen/cell wall interface, or the cell wall.[24]

It is well known that the location of the modifying agent in the wood structure has a crucial influence on the properties of the final material. As an example, the addition of hydrophobic components to wood will have different impacts on its dimensional stability according to their distribution. Native wood is subject to swelling and shrinkage due to the hygroscopic nature of the cell walls. If a hydrophobic polymer penetrates the cell wall and grafts on the cell wall hydroxyl groups, then the cell wall will be more hydrophobic, and the dimensional stability will highly increase. If the same hydrophobic polymer is now only filling up the lumen (initially a void space), then the transport of water inside wood is delayed, but it will eventually reach the unmodified cell wall. This will result in cell wall swelling and in a poor improvement of the dimensional stability.[25]

To be able to develop functional lignocellulosic materials with well-defined properties, we therefore need to control the spatial distribution of the modification. Until now, this proved to be highly challenging, because the wood structure is highly inhomogeneous, and the polymerization techniques used in wood were not selective enough. For this reason, we chose to modify wood with Surface-Initiated Atom Transfer Radical Polymerization (SI-ATRP). In general, polymer brushes can be prepared from *grafting to*, *grafting through,* or *grafting from* methods.[18,26]

For this study, a *grafting from* approach such as SI-ATRP was of particular interest. SI-ATRP has been conducted in a wide range of materials, from biological to synthetic, for various applications.[22,27–30] In this process, an initiator is first grafted onto the surface of a solid (or into the bulk of the material providing that the reagents can diffuse into it), yielding a macroinitiator. In the following step, polymer chains are grown from this covalently bonded initiator. Therefore, if the distribution of the initiator moiety can be controlled, we should be able to control the position of the grafted polymer, since the polymer chains only grow from the immobilized initiator.[31]

Although *grafting from* techniques have been applied in wood, the focus of these papers was not to show control over the polymer spatial distribution. Nevertheless, the work from Ermeydan et al. suggests that the solvent used for their Ring Opening Polymerization (ROP) approach in wood could influence the final polymer spatial distribution.[17] According to Mantanis et al.[32] the wood-swelling capability of a given solvent essentially depends on its molar volume, its basicity, and its hydrogen bonding capability.

Based on these former studies, we investigated the effect of two different solvents on the final distribution of polymers in spruce wood samples. The modifications have been carried out using surface initiated activator generated by electron transfer atomic transfer radical polymerization (SI-AGET-ATRP) technique, a modified SI-ATRP technique. We used spectroscopy techniques (FTIR and Raman) as well as electron microscopy (SEM) to provide a detailed analysis of the distributions of both the initiator and the polymer into the cell wall structure (microscale), and through the wood sample (macroscale). We found out that by using solvents with different wood-swelling capabilities (pyridine and dichloromethane), we can control the distribution of the initiator in the wood scaffold (at both micro- and macro-scales), and consequently, we can control the position of the grafted polymer.

EXPERIMENTAL SECTION

Materials. Norway spruce (*Picea abies*) was cut into cubes of $10 \times 10 \times 5\ mm^3$, Radial × Tangential × Longitudinal dimensions. Throughout the experiments, the samples used had similar earlywood/latewood distributions. Before the first functionalization step, the samples were Soxhlet extracted and dried in an oven under vacuum at 65 °C until a constant mass was reached.

Monomers [2-(Methacryloyloxy)ethyl]trimethylammonium chloride solution (METAC) and 2,2,2-Trifluoroethyl methacrylate (TFEMA), initiator α-bromoisobutyryl bromide (BiBB), reducing agent Tin(II) 2-ethylhexanoate ($Sn(Oct)_2$), copper complex $Cu(II)Br_2$, ligand N,N,N’,N’’,N’’-Pentamethyldiethylenetriamine (PMDETA), as well as solvents N,N-dimethylformamide (DMF, anhydrous grade) and dichloromethane (DCM, anhydrous grade) were purchased from Sigma-Aldrich and used as received. Pyridine (Py, anhydrous grade) was purchased from VWR and used as received.

Synthesis of wood macroinitiator. Oven dried wood samples were placed under vacuum (10^{-2} mbar) in a Schlenk flask capped with a septum. A BiBB solution (in either anhydrous Py or anhydrous DCM) was added with a syringe. When we used DCM as solvent, a small amount of pyridine was added (1:1 molar equivalent with BiBB), in order to remove the hydrogen bromide byproduct. The amounts of BiBB engaged in the reactions were calculated according to the formulas given in the Supporting Information. An example of the calculations is given in Table S1. The reaction was stirred at room temperature for a given amount of time. The reacted wood cubes were withdrawn and washed with methanol and sonicated in methanol and acetone to remove any unreacted material. After the washing, the cubes (W-Br) were dried in an oven under vacuum at 65 °C until constant mass was reached. The samples produced in this step are named W-Br(Py) and W-Br(DCM), according to the reaction solvent used.

AGET SI-ATRP of TFEMA and METAC using W-Br as macroinitiator. Both TFEMA and METAC where polymerized in DMF with the W-Br macroinitiators, using the following concentration ratio: [Monomer]:[W-Br]:[Cu(II)Br_2]:[PMDETA]:[Sn$(Oct)_2$]=10:1:1:2:2. W-Br samples were placed in a Schlenk flask, capped with a septum, together with the Cu(II)Br_2. The flask was evacuated until it reached low vacuum (ca. 10^{-2} mbar). DMF was added and the flask was placed in an oil bath at 80 °C. In a separate flask cooled with ice, ligand and monomer were dissolved in DMF. The content of the flask was sparged with nitrogen for an hour, and then added to the heated Schlenk flask containing the wood samples. The reducing agent (Sn$(Oct)_2$) was added slowly during the first 40h of polymerization using a syringe pump, and the total reaction time was 48h. The reacted wood cubes were withdrawn and washed with ethanol and sonicated in ethanol and acetone, and water for PMETAC samples, to remove any unreacted material, as well as non-grafted polymer chains. After the washing, the cubes were dried in an oven under vacuum at 65 °C until constant mass was reached. The W-Br(Py) and W-Br(DCM) samples reacted with TFEMA in this step are named W-Br(Py)-PTFEMA and W-Br(DCM)-PTFEMA, respectively. The W-Br(Py) and W-Br(DCM) samples reacted with METAC in this step are named W-Br(Py)-PMETAC and W-Br(DCM)-PMETAC, respectively.

Weight Percent Gain (WPG, %) calculation. The WPG represents the amount of modification material introduced into the cube at each modification step. To estimate the WPG, the weight of the dried wood cubes was measured before (W_{BM}) and after the modification (W_{AM}), and the WPG is calculated as follows:

$$WPG(\%) = \frac{W_{AM} - W_{BM}}{W_{BM}} * 100$$

Raman microscopy. Wood samples were polished using a rotary microtome, removing the first 200 µm of material. The measurements of the W-Br macroinitiators were performed with a confocal Raman microscope (Renishaw inVia, Wotton-under-Edge, England) using a 532 nm laser, an oil immersion objective (Nikon, 100x, NA = 1.3, 0.17 mm coverslip corrected) and an 1800 l/mm grating. As mapping parameters, an integration time of 1.5 s with circa 5 mW, and a step width of 300 nm were used. The measurements of the TFEMA and METAC polymerized samples were performed with the same Raman microscope using a 633 nm laser, a water immersion objective (Olympus, 60x, NA = 1) and a 600 l/mm grating. As mapping parameters, an integration time between 5 and 10s with circa 25 mW laser power, and a step width of 400 nm were used.

FTIR spectroscopy. Fourier transform infrared spectroscopy (FTIR) measurements were conducted on a Tensor 27 (Bruker instruments) equipped with an ATR module. One spectrum was measured every 100 µm below the wood cube surface until the cube center. This was done by slicing off 100 µm cross-sections then measuring on the fresh wood cube surface (25 spectra per cube, from 0 to 2.5 mm). Spectra were baseline-corrected with the concave rubberband correction method in the OPUS software (Bruker) and peak area normalized over the whole spectrum with MATLAB. The peak area ratios, without prior normalization, were also calculated in MATLAB.

SEM/EDX/WDX. Wood samples were polished using a rotary microtome, removing the first 200 µm of material. SEM images were obtained in an SEM FEI Quanta 200FEG. The measurements were carried out under low vacuum, at a working distance of 10 mm, with spot size of 4 and an acceleration voltage of 10 kV. The scanning electron microscopy (SEM) images were produced with a backscattered secondary electron detector (BSE).

The energy dispersive x-ray (EDX) mappings were acquired in an SEM Quanta 600 FEI. The samples were coated with a 20 nm layer of carbon prior to all measurements. The measurements were carried out under high vacuum, at a working distance of 10 mm, with a spot size of 4.5, and an acceleration voltage of 10 kV.

Wavelength dispersive x-ray (WDX) mappings were acquired in a JEOL JSM7100 FEG scanning electron microscope operating with the EDAX TEXS spectrometer. The TEXS HP is a parallel beam spectrometer (PBS) optimized to cover low energy and transition element energies from 150 eV up to 10 keV. The samples were coated with a 20 nm layer of carbon prior to all measurements. The measurements were carried out under high vacuum, at a constant working distance of 14 mm, at a spot size of 4 nA, and an acceleration voltage of 10 kV.

RESULTS AND DISCUSSION

Figure 1 illustrates the morphology of spruce wood. The year rings shown in Figure 1A are formed by a longitudinal arrangement of tracheids with different cell structures. The low-density regions are called earlywood (EW), with an average lumen size of 36 ± 7 µm and a cell wall thickness of 4 ± 0.75 µm; and the high-density regions are called latewood (LW), with an average lumen size of 8.5 ± 5.5 µm and a cell wall thickness of 5 ± 2.5 µm.[33]

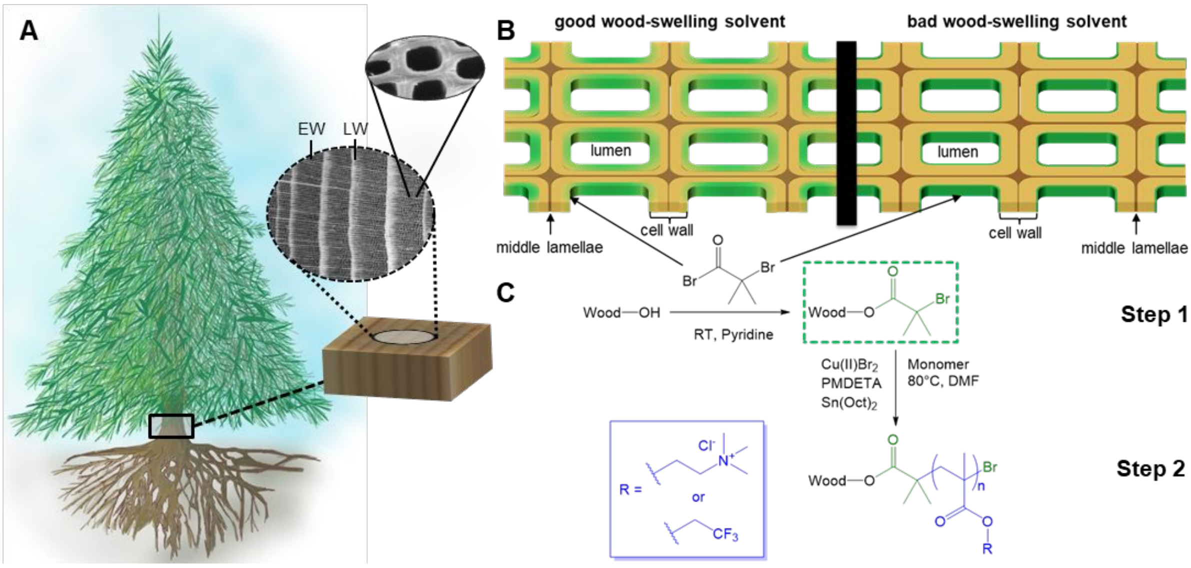

Figure 1: Scheme showing (A) the structure of spruce wood from macro- to micro-scale, (B) targeted initiator distribution into the wood structure and (C) SI-AGET-ATRP reaction process.

In most chemical wood modifications, a solvent is used to transport the reagents to the reaction sites (-OH groups). The transport of fluids in wood may occur through different pathways: from one cell to another via natural features (pits for instance), from lumen to cell wall via diffusion, and in the longitudinal direction through the middle lamellae and through cut open cell walls.[34] Although the importance of one or the other pathway is still debated, the nature of the solvent is widely accepted as a critical parameter determining the kinetics and the extent of wood impregnation and wood cell wall swelling.[32] Therefore, a possible way of controlling the distribution of chemicals in the wood structure is to use solvents with different swelling capabilities for the wood cell wall. According to the solvent system chosen, we targeted the distributions shown in Figure 1B: cell wall modification or decoration of the wood lumen/cell wall interface.

In this work, we modified wood cubes with a *grafting from* polymerization technique. SI-AGET-ATRP is a two-step reaction (see Figure 1C). In the first step, α-Bromoisobutyryl bromide (BiBB) is covalently attached to the hydroxyl groups available in the wood cell walls, to obtain the wood macroinitiator (W-Br). In the second step, the desired polymer is grown from alkyl bromide moieties present in the macroinitiator. Since the polymer chains are directly initiated at the alkyl bromide sites, the control over the distribution of the attached BiBB moieties in wood should ensure control over the final position of the polymer brushes

The interactions between wood and various organic solvents has already been investigated.[32] Based on the data provided by Mantanis et al., we selected a good and a bad wood-swelling solvent, respectively pyridine and dichloromethane, as reaction media for the esterification of wood hydroxyl groups with BiBB. By using two solvents with different wood-swelling properties, we expect to achieve two different distributions (shown in Figure 1B). In the case of pyridine, we expect to find BiBB deep inside the wood cell walls, while it should only decorate the lumen/cell wall interface in the case of dichloromethane. The swelling capability of DCM and Py were evaluated: spruce wood cubes were immersed in the two solvents, and the dimensional changes were measured. After equilibrium was reached, the cubes were swollen by 18.3% in Py, and 6.7% in DCM (see results Figure S1, in Supporting Information), thereby confirming the high swelling power of Py when compared to DCM.

Synthesis of W-Br macroinitiators: influence of reaction time, concentration, sample morphology, and solvent on the WPGs. As discussed previously, the covalent attachment of the alkyl halide compounds to the wood scaffold is a critical step for the control of the final polymer distribution. In a preliminary study, we investigated the influence of the reaction time, the BiBB concentration in solution, and the sample morphology on the final BiBB weight percent gain. As shown in Figure 2, and as reported already by Cabane et al.,[21] we observe a clear increase in WPG together with the increase of the reaction time and of the reactant's concentration.

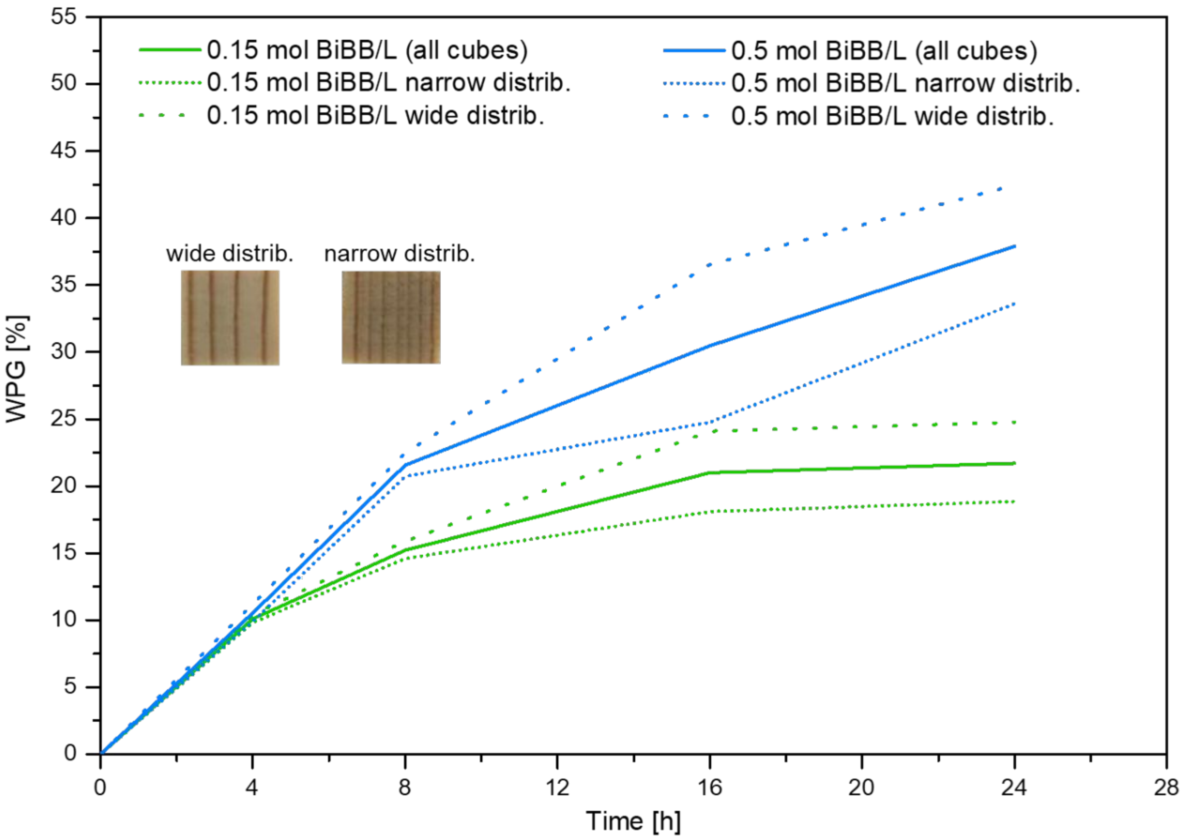

Figure 2: Evolution of WPG (%) with respect to reaction time, using different BiBB concentrations, and EW/LW distributions. For each reaction set, three samples of each year ring distributions were used. Pyridine was used as reaction media for all data sets.

More interestingly, Figure 2 shows that the macroscale morphology of the wood cubes has an effect on the final weight percent gains. The experiments were carried out using cubes with two types of wood year ring distributions In one case the cubes have a higher fraction of EW (wide year ring distribution), and in the second set of samples, more year rings are present, meaning that the fraction of LW is higher (narrow year ring distribution). According to our experiments, we obtained higher WPGs with cubes containing a higher fraction of EW. As mentioned previously, the diffusion of the pyridine solution into the cell wall is critical to ensure transport of BiBB compounds inside the cell wall, where they can react with wood hydroxyl groups. If the cell wall is thin (EW), the solution is likely to penetrate and fully swell the cell wall, providing good -OH accessibility and high WPGs. Conversely, the diffusion into thick cell walls (LW) is limited, thus a lower amount of -OH groups can be accessed, and the overall WPGs are lower. Considering these preliminary results, all reactions were performed with cubes having similar EW and LW proportions.

Finally, we investigated the effect of the solvent on the final WPG. A series of cubes were modified with two different solvents, pyridine and dichloromethane, for 20 and 24h respectively with all other conditions kept constant (room temperature, [BiBB] = 0.5 mol/L). We obtained 15% WPG for the DCM-modified cubes, and 25% WPG for the pyridine-modified cubes. We could therefore confirm that the BiBB WPG also depends on the solvent used. This was already observed by Cabane et al.,[21] and can be explained by the swelling ability of the different solvents used: a good solvent (such as pyridine) provides a better access to the wood cell wall -OH groups and subsequently a higher WPG, compared to a bad solvent system (such as DCM).

Characterization of the BiBB distribution in wood. The distribution of the alkyl bromide in the wood structure was characterized at the "microscale" (i.e. cell wall level) using SEM and Raman microscopy, and at the "macroscale" (i.e. cube level) using FTIR spectroscopy.

The microscale characterization is reported in Figure 3. Brighter areas in the SEM images correspond to the presence of elements with higher atomic weight (Br in this case), contrasting with the darker areas where elements with lower atomic weight are present (C and O – major constituents of the wood biopolymers).

The Raman images are composed by the overlap of two images obtained from the same mapping. To obtain the first image, the aromatic skeletal vibration assigned to lignin (present in the cell wall but mainly in the compound middle lamellae (CML)) was integrated (1500-1700 cm^{-1}) and is shown in red. The second image obtained from the integration of the C-Br vibration peak (270-330 cm^{-1}) and shown in green represents the distribution of the BiBB modification in the wood cell wall (the black area corresponds to the empty lumen).

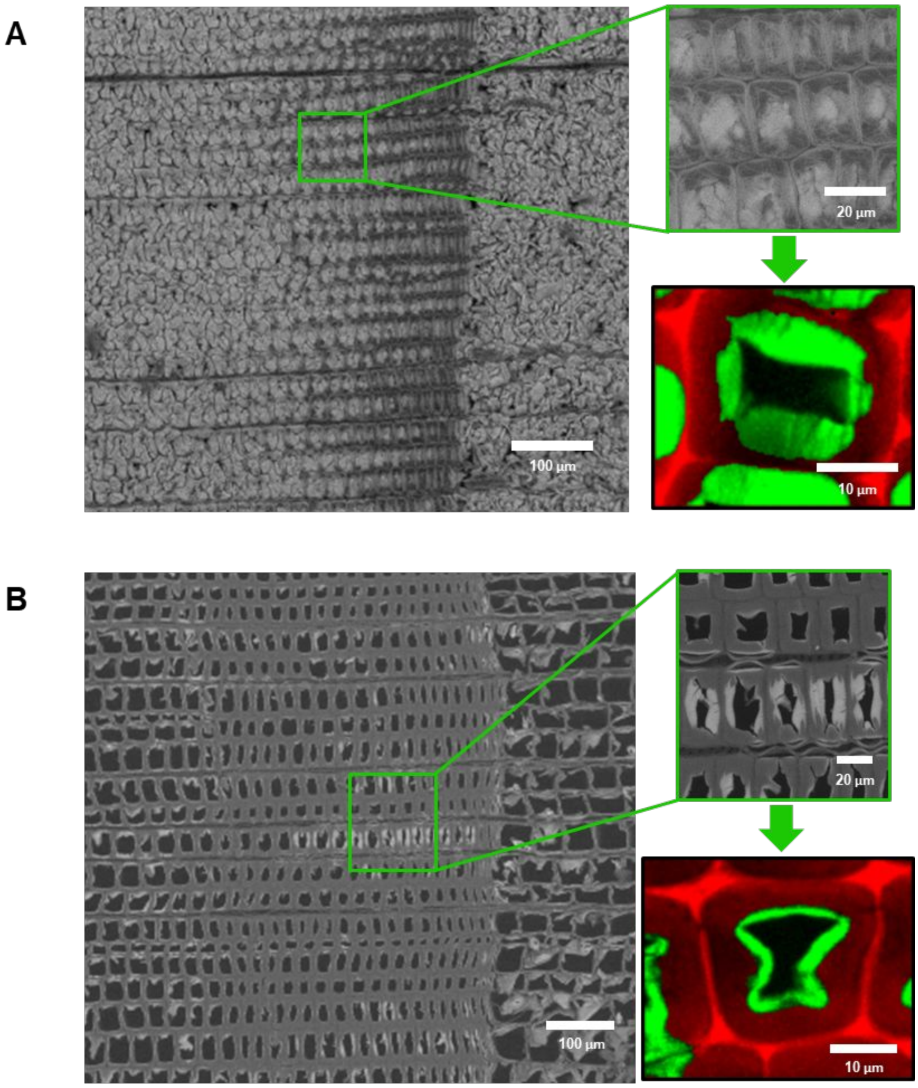

Figure 3: Raman and SEM (BSE detector) images of the BiBB distribution in the wood cell wall after modification reactions in Py (A) and DCM (B). In the Raman mappings, the green regions represent the areas modified by the initiator and in red the areas corresponding to the lignin rich regions.

The SEM (BSE) images in Figure 3A and 3B indicate that the brominated compound is distributed more homogeneously in the W-Br samples modified in pyridine. In the Raman image in Figure 3A, a large BiBB area can be observed (in green), suggesting that the modification took place deep inside the cell wall, when reacted with pyridine. In comparison, the very clear "green rim" shown in Figure 3B suggests that in the case of W-Br(DCM), the reaction was limited to the lumen/cell wall interface when reacted with dichloromethane. Both SEM and Raman images confirm that we can control the distribution of BiBB in the wood scaffold at the cell wall level with a proper choice of solvent.

The SEM images also reveal that the treatment with BiBB in both solvents alters the cell wall structures, in particular in the EW regions, where the cell walls are thin. One can easily observe that the overall cells arrangement is maintained (EW and LW regions are clearly identified), but the first layers of the cell walls can be severely damaged, with torn and swollen cell wall fragments filling up the lumen space. SEM images given in Figure S2 show that the solvents alone are not responsible for these cell wall alterations. Previous studies have shown that isolated cellulose fibers or crystals can dissolve in organic solvents when they are highly substituted (through acetylation for instance), which could explain the observed cell wall alterations.[35] However, the wood cell wall is a composite material where cellulose is not available in an isolated form: in our samples, cellulose fibers are embedded in the lignin-hemicelluloses matrix. Moreover, the calculated substitution degree for cellulose in our case is below the 0.5 critical value reported in literature (see calculations in Table S2). Therefore, we believe that the permanent cell wall alterations observed after the BiBB reaction are rather an indication that the alkyl bromide groups occupy space in the cell wall. In the most severe cases (highest BiBB WPGs obtained with Py), the extent of swelling is such that the wood cell wall structure might be disrupted. This phenomenon was already reported for other reactions in wood.[36,37] This also explains why the cell wall swelling and damage are considerably lower for the W-Br(DCM) samples, where less BiBB groups enter the cell walls.

Following the microscale investigation, we characterized the BiBB distribution at the macroscale, i.e. throughout the cubes. Penetration of liquids in wood at the macroscale is not trivial. Although the porous wood structure is designed to transport fluids over several meters, many natural openings irreversibly close upon wood felling and drying, thereby limiting transport of fluids in bulk wood materials. In our case, the geometry of the cubes is such that some tracheids will have an open end at the cube surface, but others will be entirely closed inside the bulk of the cube. Such fibers may not be fully impregnated by the BiBB solutions (regardless whether pyridine or dichloromethane is used).

To evaluate the presence of BiBB in wood at various depth, we successively removed thin cross-section slices off the cube from surface to center (i.e. from 0 to 2.5 mm), acquiring a FTIR spectrum on the fresh surface every 100 μm (see Figure 4A). For the sake of clarity, only a few spectra are shown in Figure 4B, but the ratios calculated for all depths are given in Figure 4C.

We asserted the presence of the BiBB modification through the C=O stretching signal at 1737 cm^{-1}. This carbonyl stretching is also present in native wood, but there is a pronounced increase in absorption intensity due to the presence of BiBB after the esterification.

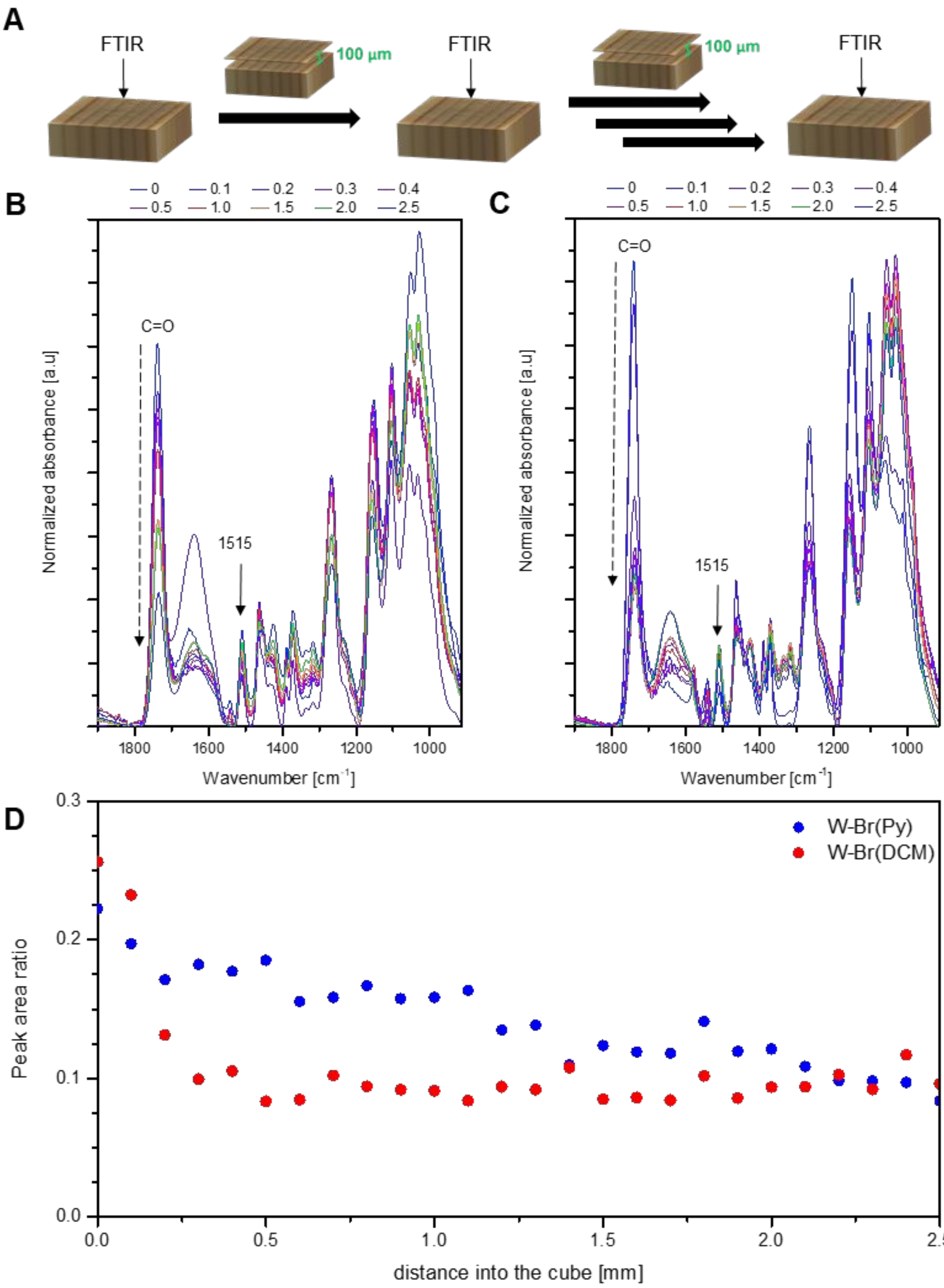

Figure 4: (A) successive removal of 100 µm thick wood slices for the FTIR study. (B) FTIR spectra of the W-Br(Py) macroinitiator at various distances from the cube surface. (C) FTIR spectra of the W-Br(DCM) macroinitiator at various distances from the cube surface. The spectra were peak area normalized through the entire spectra using MATLAB. (D) Presence of BiBB through the wood cubes shown by the ratio of the carbonyl peak area against the aromatic skeletal peak area assigned to lignin, as a function of depth.

As shown in Figure 4B and C, there is a clear decrease in the carbonyl peak intensity from the surface spectrum to the spectrum taken in the center of the cube, for both macroinitiators. This suggests that the modification is not homogeneously distributed throughout the cube, regardless of the solvent used. To facilitate the interpretation of the FTIR spectra, and because FTIR is only a semi-quantitative method, we calculated the peak area ratio between the variable carbonyl peak at 1737 cm^{-1} and the skeletal lignin peak (1515 cm^{-1}) which is not affected by the esterification (see plot in Figure 4D).[38]

For the W-Br(DCM), we see a sharp decrease in the intensity ratio immediately after the surface. This is likely due to the poor swelling capabilities of DCM, which limits the penetration of BiBB molecules inside wood, not only at the cell wall level as demonstrated earlier, but also at the macroscale. Since DCM is a bad wood-swelling solvent, it is very unlikely that the solution of BiBB can soak through several cell walls and react with the -OH groups available in the closed tracheids at the center of the cube.

Contrarily, for the samples modified with the good wood-swelling solvent, pyridine, we see that the ratio decreases regularly from the surface to the center of the cube. This indicates that the modification took place throughout the cube length, with a clear gradient in intensity. This can be explained by the ability of pyridine to swell wood cell walls, and to penetrate deep inside the wood structure. In the center of the cube (2.5 mm), the ratios for both W-Br(DCM) and W-Br(Py) are similar to ratios observed for native wood, suggesting that there is little modification taking place at this depth.

Synthesis and characterization of wood-polymer materials. Following the solvent-controlled distribution of BiBB in the wood structure, we studied the *grafting from* polymerization of two monomers using the W-Br(DCM) and W-Br(Py) macroinitiators: [2-(Methacryloyloxy)ethyl]trimethylammonium chloride solution (METAC) and 2,2,2-Trifluoroethyl methacrylate (TFEMA). METAC and TFEMA were polymerized using the same solvent, dimethylformamide (DMF). DMF is an excellent wood-swelling solvent, used to ensure that the monomers were effectively transported inside the wood samples and reached the available alkyl bromide initiating sites. Raman microscopy and SEM with EDX and WDX analysis were performed on the samples to study the distribution of these two polymers.

To analyze the distribution of the polymers at the cell wall level in the different samples, vertex component analysis (VCA) was performed in the spectral range from 200 and 1800 cm^{-1} on the respective Raman spectroscopy mappings. The analysis was performed with five endmembers for the TFEMA-modified samples and six for the METAC-modified samples. The cell wall component (CW – with contribution from lignin and cellulose), the compound middle lamellae component (CML – mainly lignin), and the modification components (W-Br-PTFEMA or W-Br-PMETAC – encompassing the spectral signatures from wood, BiBB and the corresponding polymers) are shown in Figure 5 and Figure 6. The corresponding endmember spectra are given in the corresponding figures.

In these two figures, the compound middle lamellae (CML), mainly consisting of lignin, can be clearly seen in the VCA for all the data sets. The presence of lignin is shown by the aromatic skeletal vibrations at 1607 cm^{-1}, the main lignin marker band.[39] The cell wall component (CW) can be detected by the C-C-C ring deformation at 380 cm^{-1}, or by the C-O-C glycosidic asymmetric and symmetric vibrations between 1070 and 1140 cm^{-1}, all attributed to cellulose.[39,40]

In the case of the W-Br(Py)-TFEMA samples, it is not possible to differentiate two different endmembers within the cell wall because of the overlapping of characteristic cell wall vibrations with TFEMA polymer vibrations between 1000 and 1140 cm^{-1} over the entire cell wall area. Since the VCA could not be used to identify the CW endmember for this sample, we instead produced an image of the cell wall by integrating one of the cellulose characteristic bands between 1070 and 1140 cm^{-1} (see Figure 5, image labelled with ★). Although this band also contains fluorine bands, it serves as a guidance to the position of the cell wall in the mapping.[39–41]

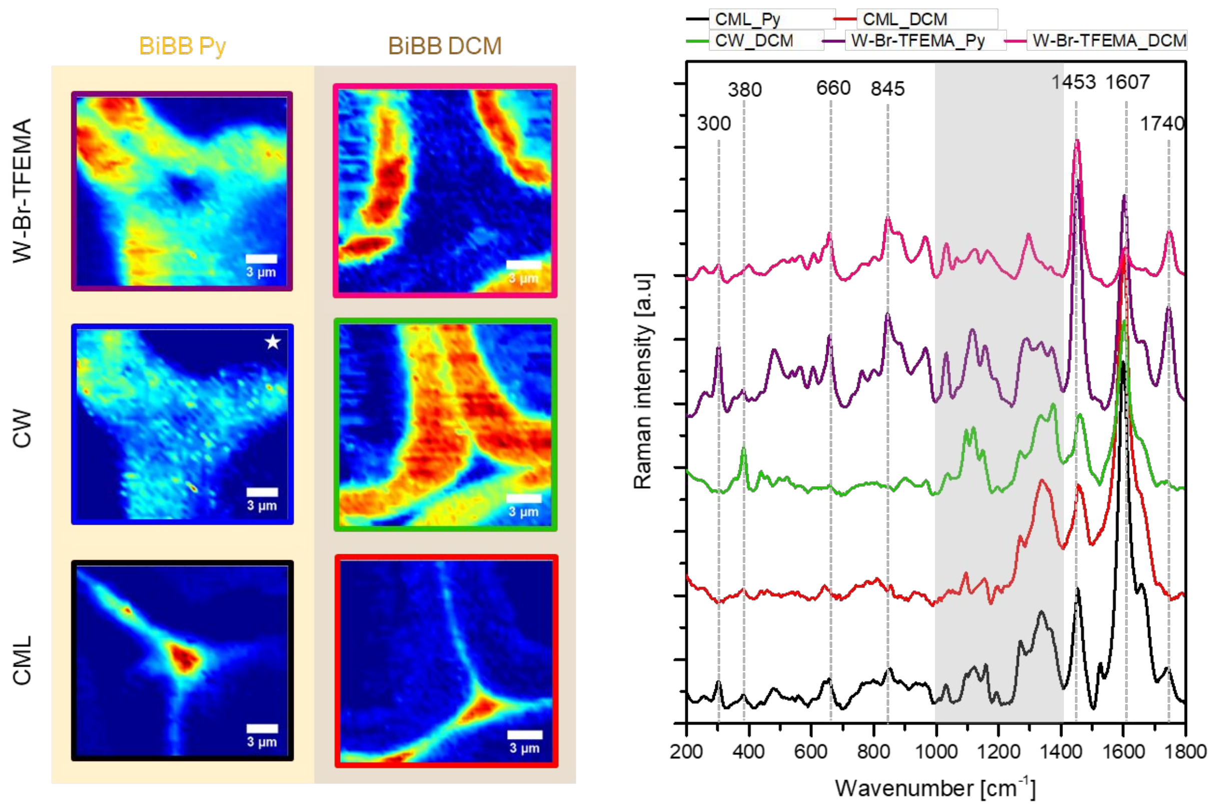

Figure 5: Raman analysis of the samples modified by PTFEMA with both W-Br(Py) and W-Br(DCM) macroinitiator sets. VCA was performed on the Raman mappings for each modification from 200 to 1800 cm^{-1}. The spectra represent the different endmembers obtained from the VCA. All images result from the VCA analysis except for the image labeled with ★, resulting from the cellulose integration (1070-1140 cm^{-1}) on the W-Br(Py)-PTFEMA sample.

To characterize PTFEMA, we used signals from the methacrylate such as the carbonyl band (C=O) at 1740 cm^{-1} and the C-CH_3 asymmetric bending band at 1453 cm^{-1}. More characteristic of the PTFEMA are several C-F vibrations bands, between 1400 and 1000 cm^{-1} and at 660 cm^{-1}, and (sat)-C-F_3 vibrations bands at both 845 and 300 cm^{-1}. [41,42]

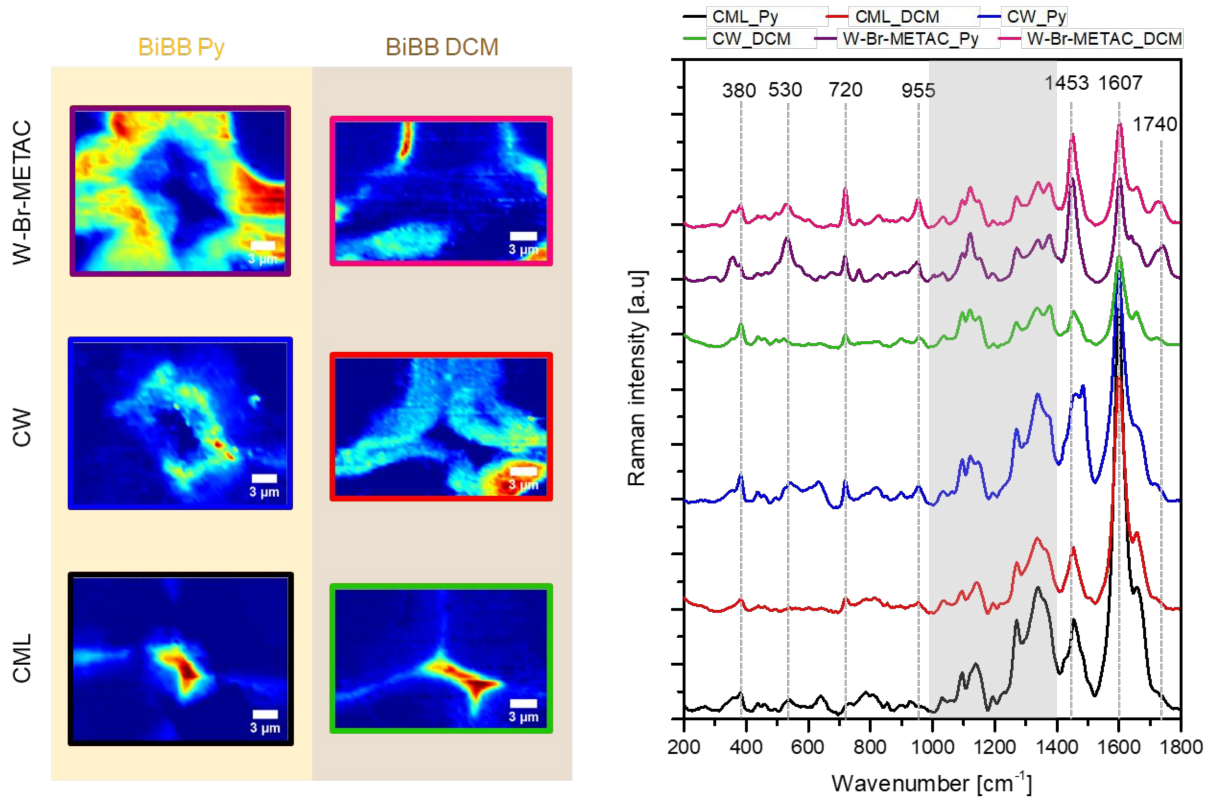

Figure 6: Raman analysis of the samples modified by PMETAC with both W-Br(Py) and W-Br(DCM) macroinitiator sets. VCA was performed on the Raman mappings for each modification from 200 to 1800 cm^{-1}. The spectra represent the different endmembers obtained from the VCA.

For the PMETAC, the characteristic methacrylate bands of the carbonyl vibration and the C-CH_3 asymmetric bending could be used again. More characteristic vibrations of PMETAC are the $N^+(CH_3)_3$ asymmetric bending at 955 cm^{-1} and the C-N symmetric stretch at 720 cm^{-1}. Vibrations from tertiary bromoalkanes from the initiator are detected at 530 cm^{-1}.[42,43]

In Figure 5 and Figure 6, respectively, it is possible to observe polymer growth deep into the cell wall structure for both polymer reactions performed on W-Br(Py) macroinitiators (W-Br(Py)-PTFEMA and W-Br(Py)-PMETAC). In the case of the set of samples obtained from the W-Br(DCM) macroinitiators, both polymer modifications (W-Br(DCM)-PTFEMA and

W-Br(DCM)-PMETAC) show a similar distribution: as opposed to the W-Br(Py)-Polymer samples, the modification is only observed at the lumen/cell wall interface.

The results obtained by Raman spectroscopy were confirmed through SEM with EDX and WDX detectors, for PTFEMA and PMETAC respectively (see Figure S3 and Figure S4, Supporting Information). The EDX results show the intensities of the Fluorine element (present in PTFEMA) throughout the cell walls for the W-Br(Py)-PTFEMA samples and at the lumen/cell wall interface for the W-Br(DCM)-PTFEMA samples.

Detecting the presence of nitrogen through X-ray energies in electron microscopy is a challenge, especially when the main scaffold mainly consists in carbon and oxygen rich polymers, due to overlapping of the nitrogen peak with the two other elements. In our samples, the nitrogen signal could not be properly detected with neither EDX nor WDX. However, in the METAC monomer, the quaternary nitrogen has a chlorine counter ion, which emits at higher x-ray energies. Using Cl, we could properly detect the presence of the PMETAC polymer. The images of the W-Br(Py)-PMETAC show the presence of chlorine inside the cell wall. In the W-Br(DCM)-PMETAC samples, chlorine may only be seen at the lumen/cell wall interface. Although this is an indirect method to detect the covalently grafted PMETAC chains, the results clearly confirm the Raman observations.

With these studies, we observed clear overlapping distributions in between the initiator and the polymers. We could therefore confirm that the polymers were grafted from the BiBB moieties anchored in the cell wall structure, regardless of the wettability properties of the monomer. These results show that it is possible to control the polymer distribution in the wood structure at the microscale.

According to the initiator WPGs and assuming that the macroscale polymer distribution at matches with the macroscale distribution of the initiator, we expected higher polymer WPGs for the samples derived from the pyridine macroinitiators. Strikingly, the results given in Table 1 show that there is no significant difference in the polymer WPGs.

Table 1: Initiator and polymer weight percent gains in the wood samples.

Sample ID	WPG BiBB [%]	WPG polymer [%]
W-Br(DCM)-PTFEMA	15.5	42.9
W-Br(Py)-PTFEMA	25.0	43.4
W-Br(DCM)-PMETAC	15.5	16.4
W-Br(Py)-PMETAC	25.0	18.4

To understand this result, we characterized the distribution of polymers at the macroscale using the FTIR method described previously for the BiBB-modified samples. To compile the graphs shown in Figure 7, we calculated the peak area ratio between the polymer signature peaks and the aromatic skeletal peak (1515 cm^{-1}), attributed to lignin. For the fluorinated polymer, the C-F signal at 1280 cm^{-1} was used, and for the PMETAC, the quaternary amine peak was used (955 cm^{-1}). The corresponding FTIR spectra can be found in Figure S5.

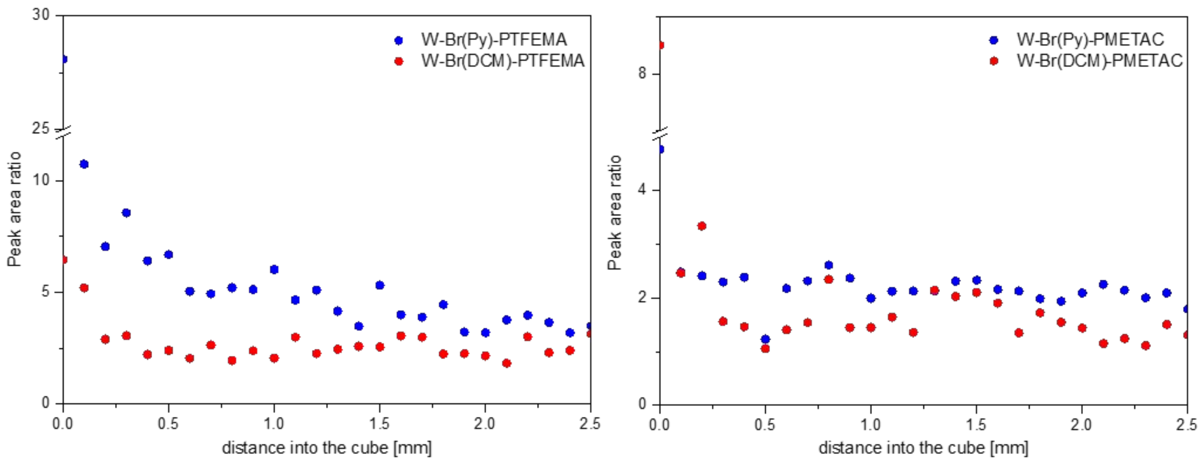

Figure 7: Macroscale distribution of the polymer modifications (TFEMA and METAC) using both W-Br(Py) and W-Br(DCM) macroinitiators. The plots show the peak area ratio between

the polymer signature peaks and the aromatic skeletal peak attributed to lignin as a function of depth.

According to Figure 7, the profiles obtained for W-Br(DCM)-PTFEMA and W-Br(DCM)-PMETAC are similar to the W-Br(DCM) profile shown in Figure 4D. Most of the polymer is present directly at the surface, then the signal drops until 300 µm, where it reaches a plateau, indicating only trace amounts of polymer in the cube center. This correlates well with the BiBB distribution obtained from the experiment in dichloromethane.

In the case of the wood-polymer samples generated from W-Br(Py) (i.e. W-Br(Py)-PTFEMA and W-Br(Py)-PMETAC), the FTIR ratio profiles do not exactly match with the W-Br(Py) profiles. Instead of the expected regular decrease seen in Figure 4D, the polymer content sharply decreases after the first cuts (500 and 200 µm below the surface for PTFEMA and PMETAC modification, respectively). Deeper into the cube, although a slight gradient is visible, low amounts of polymer modification are detected.

Therefore, regardless of the solvent used in the first modification step, the plots in Figure 7 indicate that most of the polymerization takes place at the surface of the wood cubes and in the first few hundred microns. In the end, both the W-Br(Py) and W-Br(DCM) macroinitiators generate wood-polymer materials with similar polymer distributions at the macroscale, and this explains the comparable percent gains obtained. The limited polymerization inside the wood cube likely results from a diffusion issue. The polymerization immediately starts at the wood cube surface, and the growing polymer chains will “densify” the wood surface, slowing down the penetration of the solution inside the wood bulk, and affecting the kinetics of the polymerization.

In principle, we can also estimate the chain length of the tethered polymer chains in wood. Assuming that all grafted alkyl bromide groups initiate the growth of a polymer chain, we calculated degrees of polymerization that are smaller than the targeted ones (see Table S3).

However, according to the results shown in this study, it is clear that only a fraction of the BiBB moieties actually generate polymer chains (most of the polymerization takes place close to the surface, i.e. most BiBB molecules present deep inside the wood do not react). Therefore, if we consider that no significant polymer content is found after the first 500μm (on both sides, which is consistent with the results shown in Figure 7), then we can infer that only about 20% of the cube really contains grafted polymer. If we apply this 20% correction to the fraction of BiBB reacting, we can estimate more realistic DPs, i.e. closer to the targeted DPs (see Table S3).

This table also shows that the polymerization of METAC was less controlled. Although it would need more investigations, we believe that the electrostatic interactions generated by the positively charged METAC units and growing METAC chains, as well as the positively charged ATRP catalyst could explain this observation.

CONCLUSION

We demonstrated the possibility to control the spatial distribution of the polymer chains grafted via SI-AGET-ATRP inside wood materials, using solvents with different wood-swelling capabilities. With Raman spectroscopy and SEM (BSE, EDX, WDX) we could show that a good swelling solvent (e.g. pyridine) enables the introduction of molecules such as the ATRP initiator (BiBB) deep inside the cell wall structure. Conversely, a bad swelling solvent (e.g. dichloromethane) limits the diffusion of the molecule from the lumen into the cell wall structure, resulting in modification of the lumen/cell wall interface. The control over the initiator distribution allows for the control of the polymerization of two different monomers.

In addition, we showed that the use of different solvents also allows controlling the modification distribution at the macroscale. This is particularly notable for the initiator distribution. The distribution of the polymer is somewhat less controlled, as the difference between the two W-Br-Polymer sets is less noticeable. This is due to a diffusion issue, related to the growth of the polymer chains at the surface of the wood samples. However, this issue could probably be addressed by carefully studying the kinetics of impregnation inside the wood samples.

To conclude, this study allows for a better understanding of the parameters involved in polymer modifications on wood, focusing on SI-AGET-ATRP. In many applications envisioned for functional lignocellulosic materials, the distribution of the modification is a key issue influencing the performance of the material. This study yielded important results and information for further investigations on the modification of wood, and will be of great use to design and optimize polymerization processes where a control over the distribution is needed. This will facilitate the production of wood-based materials with new functionalities for specific applications.

ASSOCIATED CONTENT

Supporting Information.

Results regarding EDX and WDX mappings of the PTFEMA and PMETAC samples in the W-Br(Py) and W-Br(DCM) sets and FTIR spectra of the corresponding modifications. Calculations for WPG, cellulose substitution degree and wood swelling experiments.

AUTHOR INFORMATION

Corresponding Author

* corresponding author: cabanee@ethz.ch

Author Contributions

The manuscript was written through contributions of all authors. All authors have given approval to the final version of the manuscript.

Funding Sources

Swiss National Science Foundation (grant no 160041).

Notes

The authors declare no competing financial interest.

ACKNOWLEDGMENT

This research work was supported by the Swiss National Science Foundation (grant no 160041). The authors are grateful to Dr. Karsten Kunze from ScopeM at ETH Zürich, for his support on the EDX measurements, and to Asel Maria Aguilar Sanchez from the IFB department at ETH Zürich for her support in the SEM measurements.

REFERENCES

(1) Chen, P.-Y.; McKittrick, J.; Meyers, M. A. Biological Materials: Functional Adaptations and Bioinspired Designs. *Prog. Mater. Sci.* **2012**, *57* (8), 1492–1704.

(2) Wegst, U. G. K.; Bai, H.; Saiz, E.; Tomsia, A. P.; Ritchie, R. O. Bioinspired Structural Materials. *Nat. Mater.* **2015**, *14* (1), 23–36.

(3) Darmanin, T.; Guittard, F. Recent Advances in the Potential Applications of Bioinspired Superhydrophobic Materials. *J. Mater. Chem. A* **2014**, *2* (39), 16319–16359.

(4) Lv, S.; Fu, F.; Wang, S.; Huang, J.; Hu, L. Novel Wood-Based All-Solid-State Flexible Supercapacitors Fabricated with a Natural Porous Wood Slice and Polypyrrole. *RSC Adv.* **2015**, *5* (4), 2813–2818.

(5) Trey, S.; Jafarzadeh, S.; Johansson, M. In Situ Polymerization of Polyaniline in Wood Veneers. *ACS Appl. Mater. Interfaces* **2012**, *4* (3), 1760–1769.

(6) Berglund, L. A.; Burgert, I. Bioinspired Wood Nanotechnology for Functional Materials. *Adv. Mater.* **2018**, *30* (19), 1–15.

(7) Okahisa, Y.; Yoshida, A.; Miyaguchi, S.; Yano, H. Optically Transparent Wood-Cellulose Nanocomposite as a Base Substrate for Flexible Organic Light-Emitting Diode Displays. *Compos. Sci. Technol.* **2009**, *69* (11–12), 1958–1961.

(8) Frey, M.; Widner, D.; Segmehl, J. S.; Casdorff, K.; Keplinger, T.; Burgert, I. Delignified and Densified Cellulose Bulk Materials with Excellent Tensile Properties for Sustainable Engineering. *ACS Appl. Mater. Interfaces* **2018**, *10* (5), 5030–5037.

(9) Zhu, M.; Song, J.; Li, T.; Gong, A.; Wang, Y.; Dai, J.; Yao, Y.; Luo, W.; Henderson, D.; Hu, L. Highly Anisotropic, Highly Transparent Wood Composites. *Adv. Mater.* **2016**, *28* (26), 5181–5187.

(10) Li, Y.; Fu, Q.; Yu, S.; Yan, M.; Berglund, L. Optically Transparent Wood from a Nanoporous Cellulosic Template: Combining Functional and Structural Performance. *Biomacromolecules* **2016**, *17* (4), 1358–1364.

(11) Vidiella del Blanco, M.; Fischer, E. J.; Cabane, E. Underwater Superoleophobic Wood Cross Sections for Efficient Oil/Water Separation. *Adv. Mater. Interfaces* **2017**, *4* (21), 1700584.

(12) Kostić, S.; Berg, J. K.; Casdorff, K.; Merk, V.; Burgert, I.; Cabane, E. A Straightforward Thiol–ene Click Reaction to Modify Lignocellulosic Scaffolds in Water. *Green Chem.* **2017**, *19* (17), 4017–4022.

(13) Wang, K.; Yiming, W.; Saththasivam, J.; Liu, Z. A Flexible, Robust and Antifouling Asymmetric Membrane Based on Ultra-Long Ceramic/Polymeric Fibers for High-Efficiency Separation of Oil/Water Emulsions. *Nanoscale* **2017**, *9* (26), 9018–9025.

(14) Cabane, E.; Keplinger, T.; Merk, V.; Hass, P.; Burgert, I. Renewable and Functional Wood Materials by Grafting Polymerization Within Cell Walls. *ChemSusChem* **2014**, *7* (4), 1020–1025.

(15) Merk, V.; Chanana, M.; Keplinger, T.; Gaan, S.; Burgert, I. Hybrid Wood Materials with Improved Fire Retardance by Bio-Inspired Mineralisation on the Nano- and Submicron Level. *Green Chem.* **2015**, *17* (3), 1423–1428.

(16) Burgert, I.; Cabane, E.; Zollfrank, C.; Berglund, L. Bio-Inspired Functional Wood-Based Materials – Hybrids and Replicates. *Int. Mater. Rev.* **2015**, *60* (8), 431–450.

(17) Ermeydan, M. A.; Cabane, E.; Hass, P.; Koetz, J.; Burgert, I. Fully Biodegradable Modification of Wood for Improvement of Dimensional Stability and Water Absorption Properties by Poly(ε-Caprolactone) Grafting into the Cell Walls. *Green Chem.* **2014**, *16* (6), 3313.

(18) Keplinger, T.; Cabane, E.; Chanana, M.; Hass, P.; Merk, V.; Gierlinger, N.; Burgert, I. A Versatile Strategy for Grafting Polymers to Wood Cell Walls. *Acta Biomater.* **2015**, *11* (1), 256–263.

(19) Furuno, T.; Imamura, Y.; Kajita, H. The Modification of Wood by Treatment with Low Molecular Weight Phenol-Formaldehyde Resin: A Properties Enhancement with

Neutralized Phenolic-Resin and Resin Penetration into Wood Cell Walls. *Wood Sci. Technol.* **2004**, *37* (5), 349–361.

(20) Rowell, R. M. *Handbook of Wood Chemistry and Wood Composites*, Second Ed.; CRC Press, 2012.

(21) Cabane, E.; Keplinger, T.; Künniger, T.; Merk, V.; Burgert, I. Functional Lignocellulosic Materials Prepared by ATRP from a Wood Scaffold. *Sci. Rep.* **2016**, *6* (1), 31287.

(22) Fu, Y.; Li, G.; Yu, H.; Liu, Y. Hydrophobic Modification of Wood via Surface-Initiated ARGET ATRP of MMA. *Appl. Surf. Sci.* **2012**, *258* (7), 2529–2533.

(23) Keplinger, T.; Cabane, E.; Berg, J. K.; Segmehl, J. S.; Bock, P.; Burgert, I. Smart Hierarchical Bio-Based Materials by Formation of Stimuli-Responsive Hydrogels inside the Microporous Structure of Wood. *Adv. Mater. Interfaces* **2016**, *3* (16), 1600233.

(24) Norimoto, M.; Gril, J.; Rowell, R. M. Rheological Properties of Chemically Modified Wood: Relationships between Dimensional and Creep Stability. *Wood Fiber Sci.* **1992**, *24* (1), 25–35.

(25) Zhang, Y.; Zhang, S. Y.; Yang, D. Q.; Wan, H. Dimensional Stability of Wood-Polymer Composites. *J. Appl. Polym. Sci.* **2006**, *102* (6), 5085–5094.

(26) Azzaroni, O. Polymer Brushes Here, There, and Everywhere: Recent Advances in Their Practical Applications and Emerging Opportunities in Multiple Research Fields. *J. Polym. Sci. Part A Polym. Chem.* **2012**, *50* (16), 3225–3258.

(27) Zampano, G.; Bertoldo, M.; Bronco, S. Poly(Ethyl Acrylate) Surface-Initiated ATRP Grafting from Wood Pulp Cellulose Fibers. *Carbohydr. Polym.* **2009**, *75* (1), 22–31.

(28) Zhang, X. M.; Ji, J. F.; Tang, Y. J.; Zhao, Y. Wood Pulp Fibers Grafted with Polyacrylamide through Atom Transfer Radical Polymerization. *Adv. Mater. Res.* **2011**, *396–398*, 1458–1461.

(29) Morits, M.; McKee, J. R.; Majoinen, J.; Malho, J.-M.; Houbenov, N.; Seitsonen, J.; Laine, J.; Gröschel, A. H.; Ikkala, O. Polymer Brushes on Cellulose Nanofibers: Modification, SI-ATRP, and Unexpected Degradation Processes. *ACS Sustain. Chem. Eng.* **2017**, *5* (9), 7642–7650.

(30) Yu, H.; Fu, Y.; Li, G.; Liu, Y. Antimicrobial Surfaces of Quaternized Poly[(2-Dimethyl Amino)Ethyl Methacrylate] Grafted on Wood via ARGET ATRP. *Holzforschung* **2013**, *67* (4), 455–461.

(31) Matyjaszewski, K.; Xia, J. Atom Transfer Radical Polymerization. *Chem. Rev.* **2001**, *101* (9), 2921–2990.

(32) Mantanis, G. I.; Young, R. A.; Rowell, R. M. Swelling of Wood Part II. Swelling in Organic Liquids. *Holzforschung* **1994**, *48* (6), 480–490.

(33) Park, Y. I.; Spiecker, H. Variations in the Tree-Ring Structure of Norway Spruce (Picea Abies) under Contrasting Climates. *Dendrochronologia* **2005**, *23* (2), 93–104.

(34) Segmehl, J. S.; Lauria, A.; Keplinger, T.; Berg, J. K.; Burgert, I. Tracking of Short

Distance Transport Pathways in Biological Tissues by Ultra-Small Nanoparticles. *Front. Chem.* **2018**, *6* (March), 1–9.

(35) Okajima, K.; Kowsaka, K.; Kamide, K. An Explanation of the Solubility Behaviour of Cellulose Acetate in Various Solvents in Terms of Supermolecular Structure Formed by Introduction of a Substituent Group into the Glucopyranose Unit. *Polym. Int.* **1992**, *29* (1), 47–59.

(36) Rowell, R. M.; Ellis, W. D. Bonding of Isocyanates to Wood. In *Urethane Chemistry and Applications*; 1981; pp 263–284.

(37) Rowell, R. M.; Gutzmer, D. I.; Sachs, I. B.; Kinney, R. E. Effects of Alkylene Oxide Treatments on Dimensional Stability of Wood. *Wood Sci.* **1976**, *9* (1), 51–54.

(38) Schwanninger, M.; Rodrigues, J. C.; Pereira, H.; Hinterstoisser, B. Effects of Short-Time Vibratory Ball Milling on the Shape of FT-IR Spectra of Wood and Cellulose. *Vib. Spectrosc.* **2004**, *36* (1), 23–40.

(39) Gierlinger, N.; Keplinger, T.; Harrington, M. Imaging of Plant Cell Walls by Confocal Raman Microscopy. *Nat. Protoc.* **2012**, *7* (9), 1694–1708.

(40) Gierlinger, N.; Keplinger, T.; Harrington, M.; Schwanninger, M. Raman Imaging of Lignocellulosic Feedstock. In *Cellulose - Biomass Conversion*; InTech, 2013; pp 159–192.

(41) Raihane, M.; Ameduri, B. Radical Copolymerization of 2,2,2-Trifluoroethyl Methacrylate with Cyano Compounds for Dielectric Materials: Synthesis and Characterization. *J. Fluor. Chem.* **2006**, *127* (3), 391–399.

(42) Socrates, G. *Infrared and Raman Characteristic Group Frequencies*; John Wiley & Sons, Ltd, 2001.

(43) Anastassopoulou, J. D. Mass and FT-IR Spectra of Quaternary Ammonium Surfactants. In *Chemistry and Properties of Biomolecular Systems*; Rizzarelli, E., Theophanides, T., Eds.; Topics in Molecular Organization and Engineering; Springer Netherlands: Dordrecht, 1991; Vol. 8, pp 1–9.

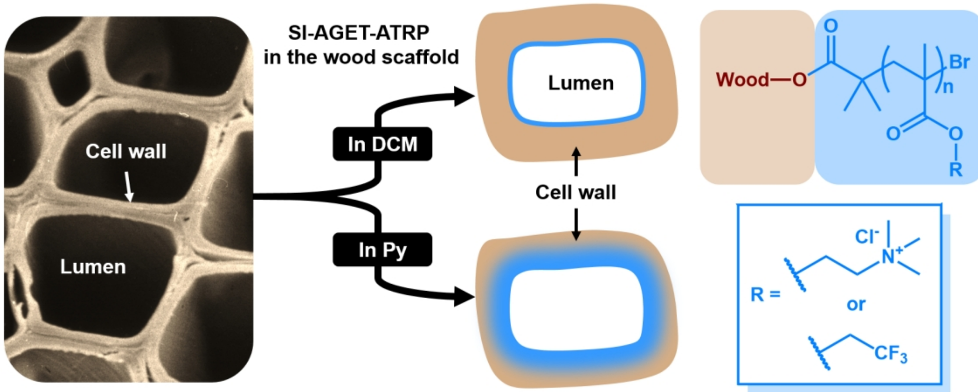

313x128mm (150 x 150 DPI)